Relevant changes in the properties of Co(Ni)Mo/Al_2O_3 HDS catalysts modified by small amounts of SiO_2

Adolfo Romero-Galarza[a)]
Departamento de Ingeniería Química, Facultad de Ciencias Químicas, Universidad Autónoma de Coahuila, Saltillo, Coahuila 25280, Mexico

Jorge Ramírez and Aída Gutiérrez-Alejandre
UNICAT, Departamento de Ingeniería Química, Facultad de Química, UNAM, Cd de México 04510, Mexico

Dora Alicia Solís-Casados
Universidad Autónoma del Estado de México, Centro Conjunto de Investigación en Química Sustentable, UAEM-UNAM, Toluca, Estado de México 50200, México

(Received 23 March 2018; accepted 10 July 2018)

The changes in hydrodesulfurization activity, selectivity, dispersion, sulfidation, and extent of promotion of Co(Ni)Mo catalysts were investigated when the alumina support surface is modified by grafting 4 wt% silica. Adding SiO_2 eliminates the most reactive hydroxyl groups on the alumina surface (IR band at 3775 cm^{-1}) decreasing the possibility of generating tetrahedral Mo species difficult to sulfide in favor of octahedral ones capable of contributing to the sulfided active phase. The catalysts were evaluated in the hydrodesulfurization of 4,6-dimethyldibenzothiophene. Incorporating SiO_2 to alumina increases the hydrogenation rate constant and therefore the global hydrodesulfurization rate of 4,6-dimethyldibenzothiophene and enhances the promotion of Mo by Co (or Ni). The global sulfidation of Ni is not affected by the addition of silica but the sulfidation of cobalt is significantly improved. The extent of promotion of the NiMo/Al_2O_3 and NiMo/SiO_2/Al_2O_3 catalysts was greater than the one achieved in their Co-promoted counterparts.

I. INTRODUCTION

In recent years, the production of more active and selective hydrodesulfurization catalysts able to remove the most refractory sulfur-containing molecules such as 4,6-dimethyldibenzothiophene has received attention due to the need to process heavier petroleum feeds, the declining trend of light oil supplies,[1] and the stringent environmental regulations requiring sulfur contents close to zero sulfur ppm in the transport fuels.

For the hydrodesulfurization of petroleum fractions, Mo or W sulfides promoted by Co or Ni supported on γ-alumina are the most extensively used catalysts.[2–6] Models for these catalysts have been proposed by Daage and Chianelli,[7] and Topsøe et al.[8] For these catalysts, complete sulfidation of the molybdenum phase leads to the so-called type II Co(Ni)–Mo–S structures that are more active than the partially sulfided type I, which strongly interact with the catalyst support via Mo–O bridges.[9,10] Type II well sulfided structures favor the presence of metallic states near the top basal plane of the MoS_2 crystallites, which can have hydrogenating properties.[9,11] Ramos et al.[12] have also shown for unsupported systems the existence of strong electron donation from Co to Mo and an enhanced metallic character associated with the Co_9S_8/MoS_2 interface. Berhault et al.[13] studied the structural role of cobalt and the influence of support interactions on the morphology and catalytic properties of Mo and CoMo catalysts supported on alumina and silica.

Development of better HDS catalysts requires to achieve (i) high dispersion of the Co(Ni)MoS active phase, (ii) complete sulfidation of the molybdenum and Co(Ni) precursor oxides phases, and (iii) high extent of promotion. It is well known that the strength of interaction between the support and the Co(Ni)–Mo supported phases has important effects on the above three parameters.

Alumina interacts strongly with the Co, Ni, and Mo oxide-supported phases, therefore, to achieve well-sulfided CoMo/Al_2O_3 and NiMo/Al_2O_3 HDS catalysts, it is necessary to modify the alumina surface with small amounts of another less interacting oxide to eliminate the most reactive alumina hydroxyl groups, which lead, during the catalyst preparation, to supported Mo oxide species difficult to reduce and sulfide. Many studies have been reported on the effect of different additives to alumina or silica to improve the catalyst performance[14–17] or to characterize the surface properties.[18,19]

Although it is known that the addition of SiO_2 to the alumina surface improves the HDS catalyst performance,[20,21] a systematic study of the changes in activity,

a)Address all correspondence to this author.
e-mail: a_romero@uadec.edu.mx
DOI: 10.1557/jmr.2018.263

selectivity, dispersion, sulfidation, and extent of promotion for CoMo and NiMo hydrodesulfurization catalysts supported on Al_2O_3 and SiO_2/Al_2O_3 has not yet been made. Accordingly, the aim of this work is to analyze how the HDS activity, selectivity, dispersion, sulfidation, and promotion of CoMo and NiMo HDS catalysts are affected by changing the nature of the catalyst support from pure Al_2O_3 to alumina grafted with 4 wt% SiO_2. The state of the supported phases is investigated by combining X-ray photoelectron spectroscopy (XPS), transmission electron microscopy (TEM), and UV-vis-diffuse reflectance spectroscopy (UV-vis-DRS). For the evaluation of activity and selectivity, the catalysts were tested in the hydrodesulfurization of 4,6-dimethyldibenzothiophene.

II. MATERIALS AND METHODS

A. Preparation of supports and catalysts

To modify the surface of the γ-alumina support with SiO_2, dry commercial γ-alumina (Sasol 2,5/210) was placed in a flask with 40 mL of anhydrous ethanol. To this solution, tetraethylorthosilicate (TEOS, 95%, Sigma-Aldrich, Saint Louis, Missouri) was added dropwise and stirred for 12 h at 78 °C. The amount of tetraethylorthosilicate was the necessary one to attain a loading of 4 wt% silica on the alumina surface. Then the solution was filtered under vacuum and the solid was dried at 100 °C for 24 h. Finally, the modified support was calcined at 550 °C for 4 h, using a heating ramp of 5 °C/min; 4 wt% SiO_2 was enough to eliminate the most basic hydroxyl groups bonded to tetrahedral aluminum (IR band at 3767 cm^{-1}),[22] as Fig. S1 shows. Hereafter, the silica-modified support is denoted as SAC.

All the catalysts were prepared with a Mo surface concentration of 2.8 Mo atoms/nm^2 and the necessary amount of Co or Ni to obtain Ni/(Ni + Mo) or Co/(Co + Mo) ratios of 0.33. The catalysts were prepared conventionally by pore volume impregnation. The alumina (Al) or SiO_2-modified alumina (SAC) supports were co-impregnated with aqueous solutions of ammonium heptamolybdate ($(NH_4)_6Mo_7O_{24}{\cdot}4H_2O$, 80% Aldrich, Saint Louis, Missouri) and nickel nitrate ($Ni(NO_3)_2{\cdot}6H_2O$, 98% Aldrich, Saint Louis, Missouri) or cobalt nitrate ($Co(NO_3)_2{\cdot}6H_2O$, 98% Aldrich, Milwaukee, Wisconsin). The impregnating solution was prepared in the following way: First, the desired amount of ammonium heptamolybdate was dissolved in 10 mL of water under agitation at 40 °C to obtain a solution of 8×10^{-5} Mo mol/mL. Then, 0.81 g of nickel nitrate or 0.82 g of cobalt nitrate was added. The pH of the resultant solution was 5. The impregnation of the support was made immediately after. At the conditions of the experiment, the solution was stable during the time of impregnation and no stabilizer was used. After impregnation, the catalysts were aged for 4 h, dried overnight at 100 °C, and calcined at 400 °C for 4 h, using a heating rate of 5 °C/min. Hereafter, the Ni- and Co-promoted catalysts supported on alumina will be named NiMoAl and CoMoAl, and their SiO_2-modified counterparts NiMoSAC and CoMoSAC.

B. Characterization of catalysts

The textural properties (specific surface area, pore volume, and pore diameter) of the catalysts were obtained using an automatic Micromeritics TriStar 3000 nitrogen physisorption instrument, Micromeritics, Norcross, Georgia. Prior to the measurements, the samples were outgassed at 270 °C for 3 h in a Micromeritics Vac Prep 061 unit, Micromeritics, Norcross, Georgia.

The UV-vis DRS spectra of oxide catalysts were taken with a Cary 500 Varian spectrometer (Cary Instruments, Mulgrave, Australia) equipped with a diffuse reflectance sphere.

FTIR spectra of Al and SAC supports were collected using a Thermo Scientific Nicolet 6700 infrared spectrophotometer (Thermo Fisher, Madison, Wisconsin) with 4 cm^{-1} resolution and 100 scans per spectrum. A self-supported sample wafer of 5 mg/cm^2 was outgassed in a special infrared cell connected to a high vacuum line. The sample was then heated at 450 °C for 2 h. Then, the sample was cooled to room temperature and the IR spectrum was collected.

A JEOL 2010 TEM (Akishima, Japan) operating at 200 kV with 1.9 Å point-to-point resolution was used for obtaining TEM micrographs of the sulfided catalysts. The samples were prepared by ultrasonically dispersing catalyst powder in heptane followed by ultrasonication for 20 min; then, a drop of the supernatant liquid was placed on a holey carbon film supported on a carbon-coated copper grid. For the statistical study of the distributions of size (length of the MoS_2 crystallites) and stacking along the *c* axis, more than 300 crystallites of each sample were measured. The software used for processing the micrographs was ImageJ.

The system used for acquisition of XPS data was a seven-channel hemispherical spectrometer (model Alpha110) of Thermo Fisher (East Grinstead, U.K.) working with a monochromatic Al-K_α source with a photo-energy of 1486.7 eV at a take-off angle of 41°, operating at 1.2×10^{-9} torr. A glove box attached to the prechamber allowed to set samples in the system without exposing them to air. Due to the nonconductive nature of the samples, a flood gun for charging compensation was used during data acquisition.

The sulfided catalysts were transported under inert atmosphere and placed into the prechamber through the glove box. Then, they were outgassed at 3×10^{-7} torr for three hours. Then, the samples were transferred to the analysis chamber. The analysis began with survey acquisition at 50 eV of pass energy and 1 eV step size,

followed by high-resolution scans of O 1*s*, Mo 3*d*, S 2*p*, Al 2*p*, and Co 2*p* and Ni 2*p* at 15 eV of pass energy and a step size of 0.1 eV. XPS data processing, including background removal and deconvolution of peaks, was performed using an interactive least-square computer program, AANALYZER® version 1.2, RDATAA (Robust Data Analysis), Chihuahua, Mexico. Prior to the analysis, shift correction of all spectra was done using Al 2*p* positioned at BE = 74.1 eV. The background was removed using Shirley–Sherwood and Shirley-Vegh-Salvi-Castle.[23]

The elemental composition (at.%) was obtained from the areas corresponding to each element in the survey spectra. Since there are several possible species for each element, the relative percent (rel.%) given in Table III of a given element is obtained by dividing its peak area by the total area formed by the different species of the same element present in the sample. For example, the relative percent of Ni in the NiMoS phase is obtained by the XPS ratio $(Ni_{NiMoS}/Ni_T)100$, where $Ni_T = Ni_{OX} + Ni_{NiMoS} + Ni_XS_Y$. The Ni atoms involved in the NiMoS phase were obtained multiplying the relative percent of Ni atoms in the NiMoS phase by the total theoretical Ni atoms divided by 100.

The elemental composition was calculated using the physical parameters described by Grant,[24] where N_A is the atomic density of the A element (proportional also to its stoichiometry), $\frac{\delta\sigma_{eA}}{\delta\Omega}$ is the photoelectric differential cross-section of the atom, evaluated considering the correction for the effect of monochromator as described by Herrera-Gomez,[25] where K_A is the photoelectron kinetic energy, λ_A is the inelastic mean free path, which was calculated using NIST Electron Inelastic-Mean-Free-Path Database (Version 1.2) National Institute of Standards and Technology, Gaithersburg, Maryland. For the calculation of the relative percent, λ_A is the effective attenuation length and was calculated using NIST Electron Effective-Attenuation-Length Database (Version 1.3) National Institute of Standards and Technology, Gaithersburg, Maryland.

$$N_A = \frac{I_A K_A}{\frac{\delta\sigma_{eA}}{\delta\Omega}\lambda_A} \quad . \tag{1}$$

C. Catalytic evaluation

Prior to the catalytic test, the catalysts were activated ex situ in a continuous flow reactor using 20 mL/min of a H_2S (15 vol%)/H_2 gas mixture at 400 °C during 4 h, with a heating ramp of 5 °C/min.

The reaction test was carried out in a batch Parr reactor operating at 320 °C and 1200 psig, using 200 mg of sulfided catalyst in 40 mL of 99%, Sigma-Aldrich, Saint Louis, Missouri containing 1000 ppm of sulfur as 97%, Aldrich, Saint Louis, Missouri. The main products from the HDS of 4,6-DMDBT were dimethyldiphenyl (DMDP), produced by the direct desulfurization route (DDS), and methylcyclohexyltoluene (MCHT) and dimethyldicyclohexyl (DMDCH), produced by the hydrogenation route (HYD). The main route of the reaction for the HDS of 4,6-DMDBT is the hydrogenation route because the direct desulfurization is sterically hindered by the presence of the methyl groups at positions 4 and 6.[26–28] This emphasizes the importance of having catalysts with an enhanced hydrogenation function. Hereafter, k_{DDS} is the rate constant for the direct desulfurization route, and k_{HYD} represents the rate constant for the hydrogenation route (see Fig. S2 in the Supplementary Material). For the calculations of the rate constants, the following equations were established:

$$r_{4,6} = dC_{4,6}/dt = -(k_{DDS} + k_{HYD})C_{4,6} \quad , \tag{2}$$

$$r_{DMDP} = dC_{DMDP}/dt = k_{DDS}C_{4,6} \quad , \tag{3}$$

$$r_{MCHT} = dC_{MCHT}/dt = k_{HYD}C_{4,6} - k_3C_{MCHT} \quad , \tag{4}$$

$$r_{DMDCH} = dC_{DMDCH}/dt = k_3C_{MCHT} \quad . \tag{5}$$

The reaction products were analyzed with an HP 6890 gas chromatograph (Wilmington, Delaware) equipped with a HP-1 column of 100 m length and 0.025 mm diameter, and a flame ionization detector. The samples of the reaction products were analyzed each hour during 6 h.

III. RESULTS AND DISCUSSION

A. Characterization of oxide catalysts

1. Nitrogen physisorption

The textural properties (specific surface area, pore diameter, and pore volume) of supports and catalysts are shown in Table I. In general, a small decrease in the specific surface area and average pore diameter is observed when silica or the metallic phases are incorporated.

2. UV-vis-DRS

To find out if the incorporation of silica to the alumina support causes changes in the coordination of the

TABLE I. Textural properties of supports and catalysts and elemental analysis.

Sample	Specific surface (m^2/g)	Average pore diameter (Å)	Average pore volume (cm^3/g)
Al_2O_3	207	92	0.55
SAC	201	74	0.54
NiMoSAC	180	72	0.45
NiMo/Al	190	67	0.43
CoMoSAC	187	58	0.62
CoMoAl	182	55	0.58

supported metals, DRS spectra of the oxide samples were obtained.

The bands due to $O^{-2} \rightarrow Mo^{6+}$ charge transfer transitions for tetrahedrally coordinated Mo^{6+} (Mo_{Td}) appear in the 210–230 nm region, while the absorption in the 250–330 nm region is ascribed to octahedrally coordinated Mo^{6+}(Mo_{Oh}).[29,30] For all the catalysts, the two absorption peaks overlapped into one (see Figs. S3(a) and S3(b) in the Supplementary Material)

The UV-spectra of the Mo oxide species in the CoMoAl catalyst showed a broad absorption band suggesting that both tetrahedral and octahedral molybdenum species are present. A mixture of tetrahedral and octahedral Mo species is also present in the NiMoAl catalyst. By contrast, for molybdenum supported on SiO_2–Al_2O_3, NiMoSAC, and CoMoSAC catalysts, a narrower absorption band shifted to lower wavelengths was present. According to Fournier et al.,[30] the position and the band width of polymolybdate species in octahedral coordination (Mo_{Oh}) are affected by the aggregate size. So, the shift of the absorption from high to low wavelength may indicate the presence of smaller well-dispersed Mo_{Td} and Mo_{Oh} species.

A doublet at 595 and 630 nm, ascribed to Ni tetrahedrally coordinated (Ni_{Td}) and an absorption at 730 nm, associated with octahedral nickel oxide species (NiO_{Oh}) are reported in the literature.[31] The DRS spectra of NiMoAl and NiMoSAC in the 500–800 nm region (see Fig. S3(c) in the Supplementary Material) and the intensities of each band are reported in Table II. The 730 nm (NiO_{Oh})/630 nm (Ni_{Td}) intensity ratio is slightly higher for NiMoSAC, indicating a slightly higher proportion of nickel octahedrally coordinated compared to NiMoAl (Table II column 5).

In the 400–800 nm region, for Co-promoted samples [Fig. S3(d) in the Supplementary Material], the addition of SiO_2 produces a decrease of the triplet with maxima at 540, 580, and 630 nm associated with cobalt tetrahedrally coordinated.[32,33] For CoMoSAC, a significant increase in the absorption bands at 450 and 750 nm associated with octahedral Co species (Co_{Oh}) is observed. The results in Table II column 7 show that the Co_{Oh} (750 nm)/Co_{Td} (580 nm) ratio is considerably higher for the CoMoSAC catalyst. Therefore, it appears that the incorporation of SiO_2 to the alumina support induces a higher proportion of octahedrally coordinated Co species. This effect is not as clear for the Ni-promoted catalyst.

B. Characterization of sulfided catalysts

1. TEM

The performance of HDS catalysts depends, among other things, on the morphology and dispersion of the active phase (MoS_2).

Micrographs of the supported MoS_2 crystallites for the series of catalysts used here can be observed in Fig. 1. All the catalysts display different slab lengths. In general, a larger population with one layer and length lower than 5 nm is observed indicating that all the catalysts present well-dispersed MoS_2 crystallites displaying the typical MoS_2 slabs with an interplanar distance of 6.1 Å.[34–36] The length and stacking distributions of the MoS_2 crystallites are presented in Fig. S4 in the Supplementary Material. NiMoAl shows shorter MoS_2 crystallites, between 21 and 40 Å, while the rest of the samples show maximum population of MoS_2 crystallite lengths between 41 and 60 Å. NiMoSAC and CoMoSAC show higher stacking than the catalysts supported on γ-alumina (NiMoAl and CoMoAl), which display mostly single layer MoS_2 crystallites.

The fraction of Mo atoms in edges and corners of the MoS_2 crystallites was estimated according to the MoS_2 hexagonal geometrical model reported by Kasztelan et al.[34] These values are reported in Table III. In general, there is little difference between NiMoAl and NiMoSAC catalysts, although the former shows slightly better dispersion. The cobalt-based catalysts show practically the same dispersion.

To enquire more on the dispersion of the catalysts and to see if the incorporation of SiO_2 to the alumina support affects the sulfidation of Mo and the formation of the so-called Ni(Co)MoS phase, XPS analysis of the sulfided samples was performed.

TABLE II. DRS-UV-Vis results; Intensity of the bands assigned to nickel and cobalt tetrahedrally and octahedrally coordinated, respectively.

	Intensity			
Catalyst	Ni_{Td} (595 nm)	Ni_{Td} (630 nm)	NiO_{Oh} (730 nm)	NiO_{Oh}/Ni_{Td} (730 nm/630 nm)
NiMoSAC	0.025	0.035	0.040	1.14
NiMoAl	0.054	0.070	0.076	1.09

	Intensity					
	Co_{Td} (540 nm)	Co_{Td} (580 nm)	Co_{Td} (630 nm)	Co_{Oh} (450 nm)	Co_{Oh} (750 nm)	Co_{Oh}/Co_{Td} (750 nm/580 nm)
CoMoSAC	0.52	0.47	0.43	0.59	0.35	0.74
CoMoAl	0.48	0.49	0.43	0.47	0.15	0.31

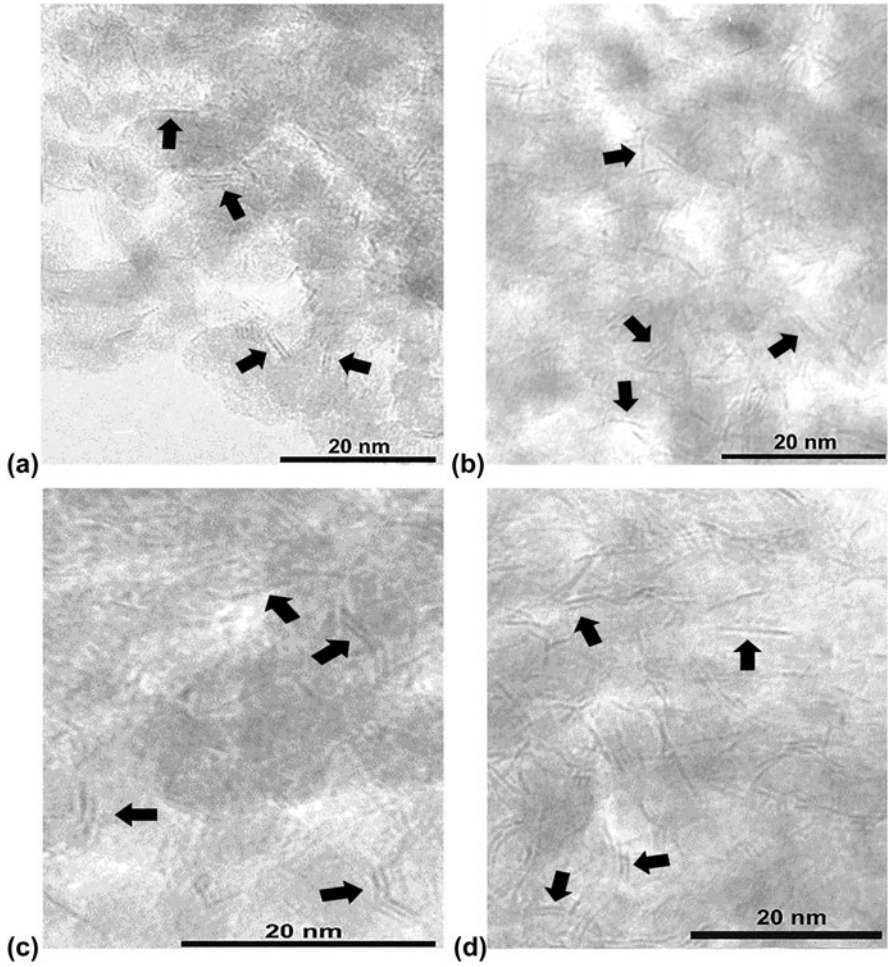

FIG. 1. TEM micrographs of sulfided catalysts (a) NiMoSAC, (b) NiMoAl, (c) CoMoSAC, and (d) CoMoAl.

TABLE III. Average length (L), average number of layers (N), and Mo distribution for MoS_2 crystallites.

Catalyst	L [Å]	N	DMo_e	DMo_C	DMo_T
NiMo/SAC	47	1.7	0.20	0.03	0.23
NiMo/Al	45	1.2	0.20	0.04	0.24
CoMo/SAC	51	1.6	0.18	0.03	0.21
CoMo/Al	55	1.5	0.18	0.02	0.20

DMo_e = Mo in edge/total Mo atoms; DMo_C = Mo in corner/total Mo; DMo_{c+e} = Mo in corner + Mo in edge/total Mo atoms.

2. XPS

XPS is a suitable technique to explore the surface properties of HDS catalysts[37–39] since it provides information on the electronic state and the distribution of the active metals on the solid surface. Concerning the modification of the alumina support surface, Table IV shows the Si/Al XPS ratio for NiMoSAC and CoMoSAC. Both catalysts have similar Si/Al ratio ~0.03, which is close to 0.035, that is, the theoretical value assuming homogeneous distribution of SiO_2 in the solid. This indicates that Si is well dispersed.

The sulfidation extent of molybdenum was estimated through the Mo^{4+}/Mo_T ratio, and the fractions of NiMoS or CoMoS promoted phases by the Ni_{NiMoS}/Ni_T or Co_{CoMoS}/Co_T ratios, respectively.

a. S-species

Three sulfur species were found on the surface of the catalysts (Table IV). A peak at ~160 eV corresponds to sulfur from sulfide phases (Ni_xS_y or Co_xS_y, respectively), that at ~162.4 eV is ascribed to S^{2-} and a small fraction of terminal S_2^{2-} of the MoS_2 phase.[38] Finally, a small peak at ~170.4 eV is assigned to sulfur from sulfate ($NiSO_4$ or $CoSO_4$, respectively).

b. Mo-species

The deconvolution of the XPS Mo 3*d*–S 2*s* spectra is shown in Fig. 2 (Only spectra of the NiMoSAC and CoMoAl samples are shown). The XPS spectra in the region of S 2*p*, Ni 2*p*, and Co 2*p* for the NiMoSAC and CoMoAl catalysts are in Fig. S5 of the Supplementary

TABLE IV. Binding energy (eV) with full width at half maximum and relative percentage of each species in sulfided catalysts.

		CoMoAl		NiMoAl		CoMoSAC		NiMoSAC	
	Peak	BE (eV) (FWHM)	Rel.%	BE (eV) (FWHM)	Rel.%	BE (eV) (FWHM)	Rel.%	BE (eV) (FWHM)	Rel.%
Mo 3*d*	MoS_2	229.8 (1.8)	83.5	230.9 (1.8)	93.5	228.8 (1.3)	82.0	229.4 (1.9)	94.3
	MoO_3	233.6 (1.8)	16.5	234.6 (1.8)	6.5	236.1 (1.8)	18.0	233.8 (1.9)	5.7
S 2*p*	MoS_2	162.9 (1.6)	75.5	163.7 (1.5)	72.2	161.3 (1.7)	60.5	162.2 (1.60)	78.2
	$Co(Ni)_xS_y$	160.2 (1.6)	17.0	161.8 (1.5)	20.7	159.7 (1.7)	28.0	160.0 (1.60)	15.4
	$Co(Ni)SO_4$	171.2 (1.6)	7.5	169.8 (1.5)	7.1	167.4 (1.7)	11.5	170.3 (1.60)	6.4
Al 2*p*	γ-alumina	74.1 (1.9)	17.9	74.1 (1.9)	18.3	74.1 (1.9)	82.6	74.1 (1.9)	21.3
	Hydroxides/oxy-hydroxides	75.6 (1.9)	82.1	75.9 (1.9)	81.7	75.6 (1.90)	17.4	75.9 (1.9)	78.7
O 1*s*	γ-alumina	528.0 (2.0)	12.9	530.1 (2.0)	30.6	531.7 (2.0)	55.5	530.2 (2.0)	20.8
	Hydroxides/oxy-hydroxides	531.7 (2.0)	54.0	532.5 (2.0)	64.0	532.5 (2.0)	44.5	531.6 (2.0)	70.6
Co 2*p*/Ni 2*p*	$Co(Ni)_xS_y$	778.4 (2.5)	16.3	853.7 (2.0)	34.2	779.0 (2.5)	24.2	853.1 (2.0)	24.8
	Co(Ni)MoS	779.4 (2.5)	21.4	854.7 (2.0)	43.2	780.0 (2.5)	37.3	854.1 (2.0)	56.6
	$Co(Ni)O_X$	782.5 (2.5)	19.4	855.8 (2.0)	10.5	783.0 (2.5)	32.3	855.4 (2.0)	18.6
	Sat1	786.1 (3.2)	11.8	860.9 (3.2)	12.1	786.6 (3.2)	3.7	...	...
	Sat2	789.0 (3.2)	10.4	...	...	789.5 (3.2)	2.5	...	...
	Loss	774.6 (3.2)	20.6	...	...	...	...	...	...

The relative percent (rel.%) corresponds to the element and not to the chemical phase.

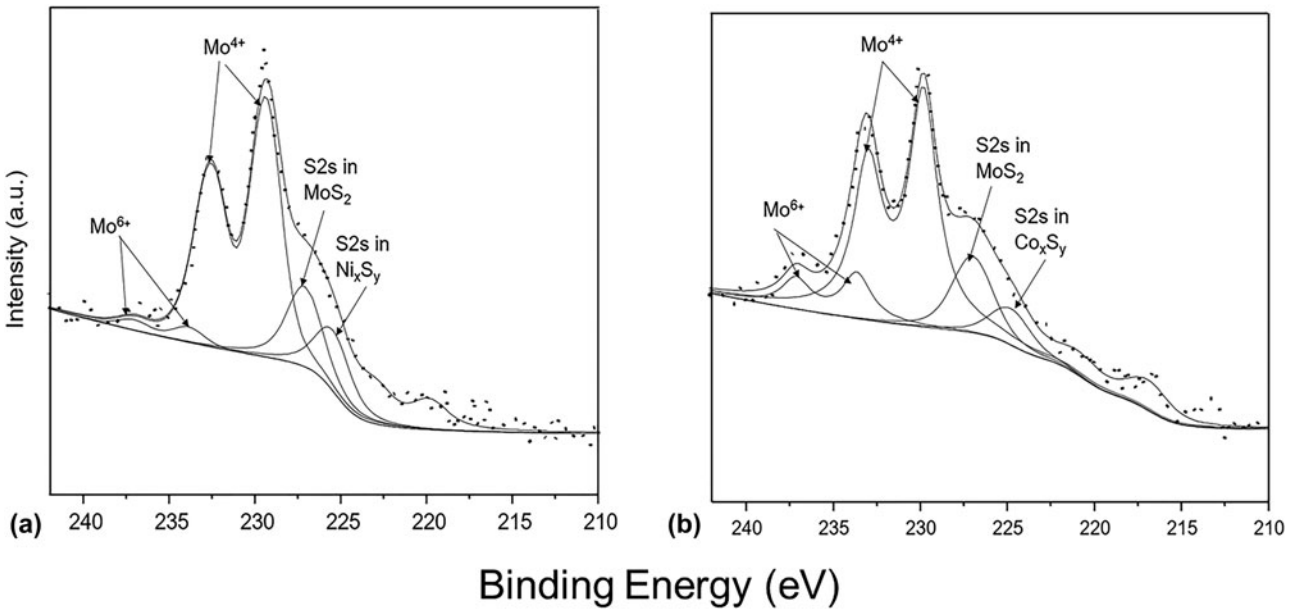

FIG. 2. XPS Mo 3*d*–S 2*s* spectra of the sulfided catalysts (a) NiMoSAC and (b) CoMoAl.

Material. All spectra were fitted with two Mo 3*d* doublets with the characteristic ratio between spin–orbit doublet of 0.66. Based on the positions of Mo $3d_{5/2}$, the BE at ~229.9 eV is associated with Mo^{4+}, which is characteristic of molybdenum sulfide (MoS_2), and Mo^{6+} at 233.6 eV characteristic of Mo in MoO_3. The binding energy values for the different atomic species reported in Table IV are in good agreement with those reported in the literature.[38,40]

c. Ni(Co)-species

The Ni 2*p* and Co 2*p* spectra for the sulfided catalysts [Figs. 3(a) and 3(c)] show that not all the Ni(Co) and Mo atoms are sulfided and contributing to the promoted Ni (Co)MoS phase.

Since Ni(Co)MoS[41] is the most active phase, it is important to determine the fraction of NiMoS or CoMoS phase in the sulfided catalysts. As reported before,[42] the Ni $2p_{3/2}$ level ascribed to the mixed NiMoS phase shows higher binding energies than nickel sulfide (853.6 eV) since the Ni atom transfers electronic density to its Mo neighbor atom.

For both core levels Ni 2*p* and Co 2*p*, the fitting was performed only in the $2p_{5/2}$ branch, using Shirley–Sherwood background subtraction. As can be seen in Fig. 3(a), the Ni 2*p* spectra for NiMoSAC was

decomposed by considering the presence of Ni_xS_y sulfide phases (Ni_2S_3, Ni_9S_8, or NiS) with binding energy at 853.1 eV, the so-called NiMoS phase with BE at 854.1 eV, and nickel oxide at 855.4 eV. Regarding nickel oxide, the BE at about 855.8 eV indicates Ni_2O_3 or Ni $(OH)_2$ but is not compatible with NiO, which presents a lower BE (~853.5 eV).

Meanwhile, the Co 2*p* spectrum was fitted considering a LMM Auger peak at 774.6 eV,[43] cobalt sulfide phases Co_xS_y like Co_2S_3, Co_9S_8, or CoS (BE at 778.4 eV),[37,44] a peak at 779.4 eV arising from the CoMoS phase, cobalt oxide (Co_{OX}) with BE at 782.5 eV, which is close to that of Co in Co_2O_3 (781.4 eV) or $Co(OH)_2$ (782 eV) but not with the BE of Co in CoO (780 eV),[12] as shown in Fig. 3(c). Finally, two satellite peaks at 786.1 eV and 789.0 eV ascribed to Co_2O_3 and Co_3O_4, respectively (see Table IV).

The quantitative analysis of the XPS results for the sulfided catalysts is summarized in Tables V and VI.

The values of the experimental Mo_T/Al ratios (Table V) indicate that Mo was better dispersed on the catalyst supported on Al_2O_3, in agreement with the DRS-UV-vis observations that show, for the oxide catalysts, the presence of relatively more Mo in tetrahedral coordination, indicating a good dispersion in the oxide state that was likely transferred to the sulfide state.

One could expect that the weaker interaction between the molybdenum species and the SiO_2–Al_2O_3 carrier (SAC) would favor a better sulfidation of molybdenum; however, the Mo^{4+}/Mo_T ratio shows that in fact, the sulfidation of molybdenum is the same for the catalysts with the same promoter and different supports, ~0.94 for NiMoSAC and NiMoAl, and of ~0.84 for CoMoSAC and CoMoAl (see Table V) indicating that, at the experimental conditions used here, the sulfidation of Mo is affected more by the type of promoter (Ni or Co) than by the type of support (Al_2O_3 or SiO_2–Al_2O_3).

Interestingly and in line with the above result, no beneficial effect of the addition of silica to alumina was observed for nickel sulfidation (Ni_S/Ni_T). However, the cobalt sulfidation ratio, Co_S/Co_T, was higher for the catalysts containing SiO_2 (see Table VI). This result could be associated with the fact that the incorporation of SiO_2, which interacts preferably with the tetrahedral centers on alumina, prevents the formation of highly stable tetrahedral cobalt species and favors the formation of octahedrally coordinated cobalt species easier to sulfide.

Other important parameters for the catalyst performance are the Ni_{NiMoS}/Ni_T, or Co_{CoMoS}/Co_T ratios, that indicate the extent of promotion.[41]

Although the Ni sulfidation degree is almost the same for the catalysts with and without Si, a higher fraction of sulfidic Ni corresponding to Ni_xS_y (Ni_2S_3, Ni_9S_8, or NiS) is present in the catalyst supported on alumina (NiMoAl) compared to NiMoSAC (see Table V column 4). On the other hand, CoMoSAC and CoMoAl have almost the same fraction of sulfidic Co associated with Co_xS_y species (Co_2S_3, Co_9S_8, or CoS) segregated from the MoS_2 phase (see Table VI column 4).

The results indicate that the incorporation of SiO_2 to the surface of Al_2O_3 enhances the formation of the NiMoS or CoMoS phases (Table V column 3). This is understandable since SiO_2 interacts with the OH alumina groups associated with tetrahedral Al, leading to a higher proportion of Mo and Co(Ni) in octahedral coordination, as the DRS-UV-vis results show for NiMoSAC and CoMoSAC. This favors the interaction between octahedral promoter and Mo species during the sulfidation step and therefore, the formation of the promoted CoMoS and NiMoS phases.

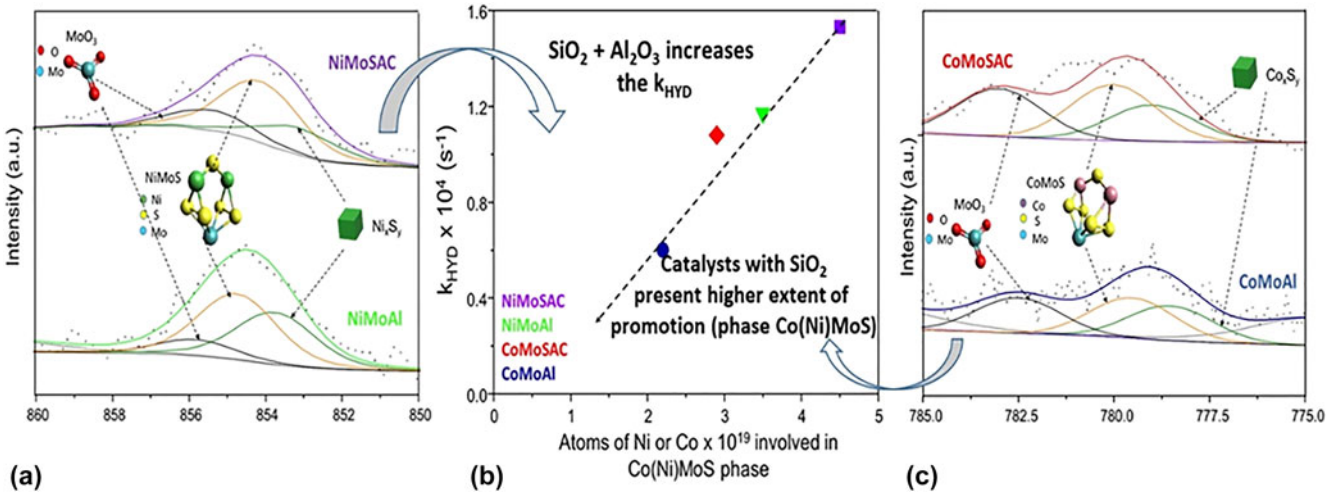

FIG. 3. (a) XPS Ni 2*p* spectra of the sulfided catalyst, (b) relationship between hydrogenation rate constant (k_{HYD}) versus Ni or Co atoms involved in the Co(Ni)MoS phase, and (c) XPS Ni 2*p* spectra of the sulfided catalyst.

TABLE V. XPS: Atomic ratio results of sulfided catalysts (400 °C/4 h).

Catalysts	NiMoSAC	NiMoAl	CoMoSAC	CoMoAl
Theoretical values				
Mo_T/Al	0.075	0.077	0.075	0.077
$Ni_T(Co_T)$/Al	0.037	0.038	0.037	0.038
$S/Mo_T+Ni_T(Co_T)$	1.75	1.75	1.75	1.75
Si/Al	0.035	...	0.035	...
Experimental values				
Mo_T/Al	0.040	0.05	0.043	0.051
$Ni_T(Co_T)$/Al	0.011	0.025	0.027	0.019
$S/Mo_T + Ni_T(Co_T)$	1.63	1.43	1.13	1.17
Si/Al	0.031	...	0.030	...
Mo^{4+}/Mo_T	0.94	0.93	0.82	0.84

TABLE VI. XPS analysis of nickel and cobalt species for sulfided catalysts.

Catalysts	Ni_S/NiT	Ni_{NiMoS}/Ni_T	Ni_xS_y/Ni_T	Ni_{OX}/Ni_T
NiMoSAC	0.8138	0.5657	0.2481	0.1861
NiMoAl	0.7737	0.4322	0.3415	0.2262
	Co_S/CoT	Co_{CoMoS}/Co_T	Co_xS_y/Co_T	Co_{OX}/Co_T
CoMoSAC	0.6151	0.3731	0.2420	0.3848
CoMoAl	0.4756	0.2700	0.2056	0.5243

Ni_S = sulfidic nickel = Ni_xS_y + Ni_{NiMoS}; Co_S = sulfidic cobalt = Co_xS_y + Co_{CoMoS}; Ni_T = total nickel = Ni_S + Ni_{NiMoS} + Ni_{OX} (oxidic nickel); Co_T = total cobalt = CoS + Co_{CoMoS} + Co_{OX} (oxidic cobalt).

The fact that the extent of promotion, Ni_{NiMoS}/Ni_T or Co_{CoMoS}/Co_T, is higher for the catalysts based on nickel than for their cobalt counterparts (see Table V column 3) can be related to the reports that indicate that NiMo catalysts can incorporate the Ni promoter on three different edges of a dodecagonal NiMoS particle, in contrast with CoMo catalysts where the Co-promoter is incorporated only on the sulfur edge of a hexagonal CoMoS cluster.[10,45]

3. Catalytic activity

a. HDS of 4,6-DMDBT

The values of the hydrodesulfurization rate constants at 320 °C and 1200 psig are shown in Table VII. The global reaction rate constant, k_{HDS}, is higher when SiO_2 is present in the catalyst and follows the order: NiMoSAC > NiMoAl and CoMoSAC > CoMoAl. There is a superiority of NiMo and CoMo catalysts supported on SiO_2–Al_2O_3 over their counterparts supported on Al_2O_3 (see Table VII).

The results in Table VII also indicate that, for the NiMo catalysts, the incorporation of SiO_2 to the support has no effect on the direct desulfurization rate constant, whereas for the CoMo catalysts, an improvement of the direct desulfurization rate constant is clear. This can be

TABLE VII. Pseudo-first-order reaction rate constants for the transformation of 4,6-DMDBT and initial HYD/DDS selectivity ratio, S_0, calculated for the batch reactor operating at T = 320 °C, P = 1200 psig.

Catalyst	$k_{HDS} \times 10^4$ (s^{-1})	$k_{HYD} \times 10^4$ (s^{-1})	$k_{DDS} \times 10^4$ (s^{-1})	$k_3 \times 10^4$ (s^{-1})	S_0
NiMoSAC	1.6384	1.5332	0.1051	0.2620	14.588
NiMoAl	1.2761	1.1717	0.1044	0.2808	11.223
CoMoSAC	1.2862	1.0808	0.2054	0.2081	5.2619
CoMoAl	0.6988	0.6015	0.0973	0.1886	6.1819

S_0 = HYD/DDS initial selectivity ratio.

associated in part with the higher extent of sulfidation and promotion achieved in the cobalt promoted catalysts supported on SAC respect to those supported on Al. The values of the rate constants and initial selectivity confirm that 4,6-DMDBT is transformed mainly by the hydrogenation reaction route. The initial reaction selectivity for the Ni-based catalysts is higher for the catalyst supported on SiO_2–Al_2O_3 than for its alumina-supported counterpart. By contrast, for the Co catalysts, the opposite occurs. This can be related in part to the higher promotion achieved for CoMoSAC that favors the DDS functionality respect to CoMoAl.

The observed raise in the hydrogenation rate constant with the addition of SiO_2 can be related to a greater population of MoS_2 crystallites with higher stacking and lower interaction with the support (Type II Co(Ni)MoS structures), as well as with an increased promotion respect to their alumina-supported counterparts (see Table VI). The good correlation between the degree of promotion with the hydrogenation rate constant displayed in Fig. 3(b), agrees with literature reports that indicate that promotion favors the appearance of brighter (more metallic) brim sites, which can perform hydrogenating reactions.[11]

The global hydrodesulfurization rate constant (k_{HDS} = k_{DDS} + k_{HYD}) is also directly proportional to the fraction of promoter atoms (Ni and Co) present in the Ni(Co)MoS phase (see Fig. S6 in the Supplementary Material), indicating that for the HDS of 4,6-DMDBT, the fraction of promoter in the Ni(Co)MoS phases not only favors the direct desulfurization route but also enhances the performance of the sites responsible for the hydrogenation route.

The better catalytic performance of NiMoSAC and CoMoSAC with respect to NiMoAl and CoMoAl can be ascribed in part to the weaker interaction between molybdenum and the SiO_2–Al_2O_3 carrier (SAC) that facilitates the formation of better sulfided Co(Ni)–Mo–S structures, favoring the formation of the sites responsible for the hydrogenation route, which is the main transformation route for the HDS of 4,6-DMDBT.

Grafting SiO_2 onto the surface of alumina has two main effects on the performance of the catalysts. One of them is to decrease the interaction of Mo, Ni, and Co with the support leading to greater availability of Ni and Co to form the mixed Ni(Co)MoS active phase (as the XPS

results show). The other effect is the elimination of the most reactive surface hydroxyl groups bonded to tetrahedral Al^{3+}, as Fig. S1 shows.[20] These hydroxyl groups are responsible for the strong interaction that leads, during the calcination of the catalyst precursors, to Co and Ni species difficult to sulfide. Therefore, grafting SiO_2 to the alumina surface leads to more Co and Ni species available to form the active phase. On the other hand, it is well known that Co favors the direct desulfurization, whereas Ni is more used to improve the hydrogenating function of the catalyst.[46] Therefore, the difference in the effect on the direct desulfurization rate constant is not only associated with the greater promotion (as the XPS results show) but also mainly to the nature of the promoter.

IV. CONCLUSIONS

For CoMo and NiMo catalysts, grafting 4.0 wt% silica on the surface of the alumina support induces better catalytic performance in the hydrodesulfurization of 4,6-DMDBT.

The global rate constant ($k_{DDS} + k_{HYD}$) for the HDS of 4,6-DMDBT correlates well with the fraction of promoter present in the Co(Ni)MoS phases, as obtained from XPS, indicating that a high level of promotion is not only beneficial to the direct desulfurization route but also improves the performance of the sites responsible for the hydrogenation route.

The addition of SiO_2 to the alumina support does not affect the degree of sulfidation of Mo (estimated as the Mo^{4+}/Mo_T ratio), which is mostly affected by the type of promoter with Ni inducing a larger value of the Mo^{4+}/Mo_T ratio.

The global sulfidation of the Ni species, estimated as the Ni_S/Ni_T ratio, is not affected by the addition of silica to the alumina support, but the sulfidation of cobalt is significantly improved. This can be related to the greater amount of tetrahedral Co species, difficult to sulfide, formed over alumina, which diminish when SiO_2 is incorporated.

The extent of promotion (Ni_{NiMoS}/Ni_T) is larger for the Ni-promoted catalysts, in line with the fact that Ni compared to Co can promote a greater number of edges in the MoS_2 nanoparticles.

The better performance of the NiMoSAC and CoMoSAC catalysts over their alumina-supported counterparts, NiMoAl and CoMoAl, seems to be mainly related to the higher extent of promotion and sulfidation achieved in the catalysts with SiO_2, fact that is reflected in a greater rate constant for the hydrogenation route, which is the main transformation route for the HDS of 4,6-DMDBT.

ACKNOWLEDGMENTS

Adolfo-Romero Galarza acknowledges postdoctoral grant from CONACyT. We acknowledge financial support from DGAPA-UNAM, project PAPIIT-IN-113015. We thank Mariela Bravo-Sanchez (Universidad de Guadalajara) for her discussion about the XPS results, Ivan Puente for the TEM work, and Alberto Herrera-Gómez (CINVESTAV-Unidad Querétaro, Mexico) for providing computer program AANALYZER® version 1.2.

REFERENCES

1. ENI (2016). Available at: https://www.eni.com/docs/en_IT/enicom/company/fuel-cafe/WOGR-2016.pdf (accessed June 19, 2018).
2. C. Song: An overview of new approaches to deep desulfurization for ultra-clean gasoline, diesel fuel and jet fuel. *Catal. Today* **86**, 211 (2003).
3. I.I. Abu and K.J. Smith: HDN and HDS of model compounds and light gas oil derived from Athabasca bitumen using supported metal phosphide catalysts. *Appl. Catal., A* **328**, 58 (2007).
4. A. Stanislaus, A. Marafi, and M.S. Rana: Recent advances in the science and technology of ultra low sulfur diesel (ULSD) production. *Catal. Today* **153**, 1 (2010).
5. A. Villarreal, J. Ramírez, L.C. Caero, P.C. Villalón, and A. Gutiérrez-Alejandre: Importance of the sulfidation step in the preparation of highly active $NiMo/SiO_2/Al_2O_3$ hydrodesulfurization catalysts. *Catal. Today* **250**, 60 (2015).
6. S. Ren, J. Li, B. Feng, Y. Wang, W. Zhang, G. Wen, Z. Zhang, and B. Shen: A novel catalyst of Ni, W-surface-Ti-rich-ETS-10/Al_2O_3 : Its role and potential of HDS performance for steric hindered sulfur compound 4,6-DMDBT. *Catal. Today* **263**, 136 (2016).
7. M. Daage and R.R. Chianelli: structure-function relations in molybdenum sulfide catalysts: The Rim-Edge Model. *J. Catal.* **149**, 414 (1994).
8. H. Topsoe: In situ Mossbauer emission spectroscopy studies of unsupported and supported sulfided Co–Mo hydrodesulfurization catalysts: Evidence for and nature of a Co–Mo–S phase. *J. Catal.* **68**, 433 (1981).
9. B. Hinnemann, J.K. Nørskov, and H. Topsøe: A density functional study of the chemical differences between type I and type II MoS_2 -based structures in hydrotreating catalysts. *J. Phys. Chem. B* **109**, 2245 (2005).
10. H. Topsøe: The role of Co–Mo–S type structures in hydrotreating catalysts. *Appl. Catal., A* **322**, 3 (2007).
11. F. Besenbacher, M. Brorson, B.S. Clausen, S. Helveg, B. Hinnemann, J. Kibsgaard, J.V. Lauritsen, P.G. Moses, J.K. Nørskov, and H. Topsøe: Recent STM, DFT, and HAADF-STEM studies of sulfide-based hydrotreating catalysts: Insight into mechanistic, structural and particle size effects. *Catal. Today* **130**, 86 (2008).
12. M. Ramos, G. Berhault, D.A. Ferrer, B. Torres, and R.R. Chianelli: HRTEM and molecular modeling of the MoS_2–Co_9S_8 interface: Understanding the promotion effect in bulk HDS catalysts. *Catal. Sci. Technol.* **2**, 164 (2012).
13. G. Berhault, M. Perez De la Rosa, A. Mehta, M.J. Yácaman, and R.R. Chianelli: The single-layered morphology of supported MoS_2-based catalysts—The role of the cobalt promoter and its effects in the hydrodesulfurization of dibenzothiophene. *Appl. Catal., A* **345**, 80 (2008).
14. M. Breysse, P. Afanasiev, C. Geantet, and M. Vrinat: Overview of support effects in hydrotreating catalysts. *Catal. Today* **86**, 5 (2003).
15. J. Xu, T. Huang, and Y. Fan: Highly efficient $NiMoSiO_2$–Al_2O_3 hydrodesulfurization catalyst prepared from gemini surfactant-dispersed Mo precursor. *Appl. Catal., B* **203**, 839 (2017).
16. A.V. da Silva Neto, E.R. Leite, V.T. da Silva, J.L. Zotin, and E.A. Urquieta-González: NiMoS HDS catalysts—The effect of the Ti and Zr incorporation into the silica support and of the catalyst

preparation methodology on the orientation and activity of the formed MoS_2 slabs. *Appl. Catal., A* **528**, 74 (2016).
17. J. Il Park, K. Nakano, Y.K. Kim, J. Miyawaki, S.H. Yoon, and I. Mochida: Characteristics on HDS over amorphous silica–alumina in single and dual catalytic bed system for gas oil. *Catal. Today* **164**, 100 (2011).
18. M. Caillot, A. Chaumonnot, M. Digne, C. Poleunis, D.P. Debecker, and J.A. Van Bokhoven: Synthesis of amorphous aluminosilicates by grafting: Tuning the building and final structure of the deposit by selecting the appropriate synthesis conditions. *Microporous Mesoporous Mater.* **185**, 179 (2014).
19. A.R. Mouat, C. George, T. Kobayashi, M. Pruski, R.P. Van Duyne, T.J. Marks, and P.C. Stair: Highly dispersed SiO_x/Al_2O_3 catalysts illuminate the reactivity of isolated silanol sites. *Angew. Chem., Int. Ed.* **54**, 13346 (2015).
20. F. Sánchez-Minero, J. Ramírez, A. Gutiérrez-Alejandre, C. Fernández-Vargas, P. Torres-Mancera, and R. Cuevas-Garcia: Analysis of the HDS of 4,6-DMDBT in the presence of naphthalene and carbazole over $NiMo/Al_2O_3–SiO_2(x)$ catalysts. *Catal. Today* **133–135**, 267 (2008).
21. C. Fernández-Vargas, J. Ramírez, A. Gutiérrez-Alejandre, F. Sánchez-Minero, R. Cuevas-García, and P. Torres-Mancera: Synthesis, characterization and evaluation of $NiMo/SiO_2–Al_2O_3$ catalysts prepared by the pH-swing method. *Catal. Today* **130**, 337 (2008).
22. G. Busca, V. Lorenzelli, G. Ramis, and R.J. Willey: Surface sites on spinel-type and corundum-type metal oxide powders. *Langmuir* **9**, 1492 (1993).
23. A. Herrera-Gomez, M. Bravo-Sanchez, O. Ceballos-Sanchez, and M.O. Vazquez-Lepe: Practical methods for background subtraction in photoemission spectra. *Surf. Interface Anal.* **46**, 897 (2014).
24. J.T. Grant: Methods for quantitative analysis in XPS and AES. *Surf. Interface Anal.* **14**, 271 (1989).
25. A. Herrera-Gomez: Effect of monochromator X-ray Bragg reflection on photoelectric cross section. *J. Electron Spectrosc. Relat. Phenom.* **182**, 81 (2010).
26. D. Duayne whitehurst, T. Isoda, and I. Mochida: Present state of the art and future challenges in the hydrodesulfurization of polyaromatic sulfur compounds. *Adv. Catal.* **42**, 345 (1998).
27. M. Egorova and R. Prins: Competitive hydrodesulfurization of 4,6-dimethyldibenzothiophene, hydrodenitrogenation of 2-methylpyridine, and hydrogenation of naphthalene over sulfided $NiMo/\gamma\text{-}Al_2O_3$. *J. Catal.* **224**, 278 (2004).
28. F. Sánchez-Minero, J. Ramírez, R. Cuevas-Garcia, A. Gutierrez-Alejandre, and C. Fernández-Vargas: Kinetic study of the HDS of 4,6-DMDBT over $NiMo/Al_2O_3–SiO_2(x)$ catalysts. *Ind. Eng. Chem. Res.* **48**, 1178–1185 (2009).
29. R.S. Weber: Weber-Effect of locat structure UV-vis absorption edges of Mo oxides.pdf. *J. Catal.* **151**, 470 (1995).
30. M. Fournier, C. Louis, M. Che, P. Chaquin, and D. Masure: Polyoxometallates as models for oxide catalysts. Part I. An UV-visible reflectance study of polyoxomolybdates: Influence of polyhedra arrangement on the electronic transitions and comparison with supported molybdenum catalysts. *J. Catal.* **119**, 400 (1989).
31. R.A. Viscarra Rossel, R.N. McGlynn, and A.B. McBratney: Determining the composition of mineral-organic mixes using UV-vis-NIR diffuse reflectance spectroscopy. *Geoderma* **137**, 70 (2006).
32. A. Stranick, M. Houalla, and D.M. Hercules: The effect of boron on the state and dispersion catalysts of $Co/A1_2O_3$. *J. Catal.* **104**, 396 (1987).
33. J.E. Herrera, L. Balzano, A. Borgna, W.E. Alvarez, and D.E. Resasco: Relationship between the structure/composition of Co–Mo catalysts and their ability to produce single-walled carbon nanotubes by CO disproportionation. *J. Catal.* **204**, 129 (2001).
34. S. Kasztelan, H. Toulhoat, J. Grimblot, and J.P. Bonnelle: A geometrical model of the active phase of hydrotreating catalysts. *Appl. Catal.* **13**, 127 (1984).
35. E. Payen, R. Hubaud, S. Kasztelan, O. Poulet, and J. Grimblot: Morphology of MoS_2 HREM study. *J. Catal.* **147**, 123 (1994).
36. E.J.M. Hensen, P.J. Kooyman, Y. Van der Meer, A.M. Van der Kraan, V.H.J. De Beer, J.A.R. Van Veen, R.A. Van Santen, E.J.M. Hensen, P.J. Kooyman, Y. Van der Meer, and A.M. Van der Kraan: The relation between morphology and hydrotreating activity for supported MoS_2 particles. *J. Catal.* **199**, 224 (2001).
37. J.A. Toledo-Antonio, M.A. Cortés-Jácome, C. Angeles-Chávez, J. Escobar, M.C. Barrera, and E. López-Salinas: Highly active CoMoS phase on titania nanotubes as new hydrodesulfurization catalysts. *Appl. Catal., B* **90**, 213 (2009).
38. L. Qiu and G. Xu: Peak overlaps and corresponding solutions in the X-ray photoelectron spectroscopic study of hydrodesulfurization catalysts. *Appl. Surf. Sci.* **256**, 3413 (2010).
39. H. Li, M. Li, Y. Chu, F. Liu, and H. Nie: Essential role of citric acid in preparation of efficient NiW/Al_2O_3 HDS catalysts. *Appl. Catal., A* **403**, 75 (2011).
40. S. Damyanova, L. Petrov, and P. Grange: XPS characterization of zirconium-promoted CoMo hydrodesulfurization catalysts. *Appl. Catal., A* **239**, 241 (2003).
41. A.S.S. Walton, J.V.V. Lauritsen, H. Topsøe, and F. Besenbacher: MoS_2 nanoparticle morphologies in hydrodesulfurization catalysis studied by scanning tunneling microscopy. *J. Catal.* **308**, 306 (2013).
42. Z. Le, P. Afanasiev, D. Li, X. Long, and M. Vrinat: Solution synthesis of the unsupported Ni–W sulfide hydrotreating catalysts. *Catal. Today* **130**, 24 (2008).
43. D. Cabrera-German, G. Gomez-Sosa, and A. Herrera-Gomez: Accurate peak fitting and subsequent quantitative composition analysis of the spectrum of Co 2*p* obtained with Al K_α radiation: I: Cobalt spinel. *Surf. Interface Anal.* **48**, 252 (2016).
44. Y. Okamoto and T. Kubota: A model catalyst approach to the effects of the support on Co–Mo hydrodesulfurization catalysts. *Catal. Today* **86**, 31 (2003).
45. J.V. Lauritsen, J. Kibsgaard, G.H. Olesen, P.G. Moses, B. Hinnemann, S. Helveg, J.K. Nørskov, B.S. Clausen, H. Topsøe, E. Lægsgaard, and F. Besenbacher: Location and coordination of promoter atoms in Co- and Ni-promoted MoS_2-based hydrotreating catalysts. *J. Catal.* **249**, 220 (2007).
46. S.L. González-Cortés: Comparing the hydrodesulfurization reaction of thiophene on $\gamma\text{-}Al_2O_3$ supported CoMo, NiMo, and NiW sulfide catalysts. *React. Kinet. Catal. Lett.* **97**, 131 (2009).

Supplementary Material

To view supplementary material for this article, please visit https://doi.org/10.1557/jmr.2018.263.